Ultrasonics Sonochemistry 73 (2021) 105497

Contents lists available at ScienceDirect

Ultrasonics Sonochemistry

journal homepage: www.elsevier.com/locate/ultson

Short communication

Understanding the relationship between particle size and ultrasonic treatment during the synthesis of metal nanoparticles

Guannan Yang [a,b,1], Wei Lin [a,1], Haiqi Lai [a], Jin Tong [a], Junjun Lei [a], Maodan Yuan [a], Yu Zhang [a,b,*], Chengqiang Cui [a,b,*]

[a] State Key Laboratory of Precision Electronic Manufacturing Technology and Equipment, Guangdong University of Technology, Guangzhou 510006, PR China
[b] Jihua Laboratory, Foshan 528225, PR China

ARTICLE INFO

Keywords:
Metal nanoparticles
Ultrasonic treatment
Wet-chemical redox method
Size refinement

ABSTRACT

Ultrasonic treatment is an effective method for size refinement and dispersion of nanomaterials during their synthesis process. However, the quantitative relationship between ultrasonic conditions and particle size in the synthesis of metal nanoparticles has not been fully revealed. In this study, Cu nanoparticles were synthesized via the wet-chemical redox method under ultrasonic treatment, and statistical analysis on the evolution of particle size distribution was carried out. It was found that the particle size decreased exponentially with increasing ultrasonic power. A quantitative model was then proposed to describe the influence of ultrasonic power on the size distribution of metal nanoparticles from the perspective of the competition between the surface energy and the ultrasonic force. A relational expression of $R_c \propto \gamma^{\frac{4}{7}} P^{-\frac{3}{7}}$ was revealed, and it was proved to fit well with the experimental results. Our study provides new experimental basis and theoretical method for understanding the mechanism of ultrasonic-induced size refinement of metal nanoparticles.

1. Introduction

Due to their high specific surface area and surface energy, nanomaterials possess a series of special properties such as low melting point, high catalytic activity, antibacterial properties, and good photosensitivity [1–6]. In the past decades, nanomaterials have been widely applied in the fields of catalysis, microelectronic packaging, ceramics, and metallurgy [7–10]. Since the properties of nanomaterials are sensitive to the size and shape, it has become a key issue to control the size and morphology in the synthesis of nanomaterials. However, owing to their small particle size, nanomaterials can easily form aggregations or agglomerations, which may cause serious deterioration of their properties. In view of this, ultrasonic treatment is introduced as an effective method to synthesize dispersed nanomaterials with fine particles or grains [11–13]. Compared with the bead milling method and other synthesis methods by virtue of magnetic field, electric field, optical tweezers, or fluidic separation [14–16], ultrasonic treatment shows many advantages such as high frequency, good directionality and transmissibility, high energy concentration, strong reflectivity, and easy availability. So far, ultrasonic treatment has been widely used in the synthesis of different kinds of nanomaterials and their composites, including metal nanoparticles, colloidal sols, catalytic materials, and proteins [7,8,17,18]. Bozkurt introduced ultrasonic treatment to the synthesis of Ag/graphene nanocomposites, and successfully prepared spherical Ag nanoparticles with an average particle size of 19.9 ± 4.9 nm [11]. Lv et al. applied ultrasound radiation to the precipitation reaction of Cu-salt and $Al(NO_3)_3{\cdot}9H_2O$, and obtained mono-phasic copper aluminate with a crystallite size of 17 nm [13]. Zhao et al. applied ultrasonic treatment during the solidification process of Al-7Si melt containing nano-sized TiB_2 particles, and the grain size of α-Al phase could be significantly reduced from 500 to 60 μm [19]. Roshini et al. introduced ultrasonic treatment to the synthetic process of graphite-reinforced Al matrix, and reduced the size of graphite flakes to 100–120 nm, along with an improvement of the porosity and distribution of graphite particles [20]. Sabnis et al. investigated the influences of ultrasonic power and ultrasonic probe shape on the productivity and size of recrystallized 3,3′-Diamino Diphenyl Sulfone (DADPS), and found a decreasing trend of particle size with the increase of ultrasonic power

* Corresponding authors at: State Key Laboratory of Precision Electronic Manufacturing Technology and Equipment, Guangdong University of Technology, Guangzhou 510006, PR China.
E-mail addresses: zhangyu@gdut.edu.cn (Y. Zhang), cqcui@gdut.edu.cn (C. Cui).
[1] The authors contributed equally to this work.

https://doi.org/10.1016/j.ultsonch.2021.105497
Received 7 December 2020; Received in revised form 2 February 2021; Accepted 15 February 2021
Available online 20 February 2021

density [21]. Shi et al. used the ultrasound-assisted precipitation method to prepare Ni/Al_2O_3 catalyst, and the particle size was reduced from 13.91 to 6.79 μm by ultrasound treatment, which greatly improved the catalytic activity [7].

Despite the wide applications of ultrasonic treatment, the influencing mechanism of ultrasound on the size and dispersibility of particles is still poorly understood. In the synthesis of metal nanoparticles, depending on different material systems, reaction mechanisms, experimental conditions, dispersants, and other additives in the solution, the size of as-synthesized particles can vary widely from a few nanometers to the micron scale [19]. Some studies reported that ultrasonic treatment could be applied to synthesize nanoparticles [11,13,22], whereas some studies showed that the size of the particles maintained at 10 μm and could not be further reduced by further increasing the ultrasound power from a certain value [21]. In general, the mechanism of particle refinement by ultrasound can be qualitatively understood based on the acoustic radiation force and ultrasonic cavitation effect [21,23,24]. However, for the synthesis of metal nanoparticles, the quantitative relationship between ultrasonic conditions and particle size has not been fully revealed.

On account of this, we carried out statistical analysis on the evolution of size distribution of Cu nanoparticles synthesized via the wet-chemical redox method under ultrasonic treatment in a power range from 0 to 500 W. The results showed that ultrasonic treatment could significantly reduce the average particle size and the size variation. An exponential relationship between the particle size and the ultrasonic power was revealed, and a model was then proposed to quantitatively describe the influence of ultrasonic treatment on the size refinement of the Cu nanoparticles from the perspective of the competition between the surface energy and the ultrasonic force. On this basis, a relational expression between the particle size and the ultrasonic power was established. It was proved that the relational expression fitted well with the experimental results.

2. Experimental

Copper acetate ($Cu(CH_3COO)_2$, analytical grade, 99.9%) and ascorbic acid ($C_6H_8O_6$) were purchased from Aladdin Biochemical Technology Co., Ltd. Ethylene glycol ($(CH_2OH)_2$) was purchased from Sinopharm Chemical Reagent Co., Ltd. All chemicals were used as received without further purification. Cu nanoparticles were prepared by the wet-chemical redox method. 0.1 mol/L $Cu(CH_3COO)_2$ and 0.4 mol/L $C_6H_8O_6$ were dissolved in two absolute ethylene glycol solutions with the same volume of 50 mL. After the solutes were completely dissolved, the two solutions were mixed in a KQ5200DE ultrasonic instrument. The volume of the stainless-steel ultrasonic reactor was 300 mm × 240 mm × 150 mm. Ultrasound was emitted evenly from the bottom of this reactor. The excitation frequency was set as 40 kHz. Different ultrasonic powers of 80, 120, 160, 200, and 500 W were applied for investigation. Correspondingly, the ultrasonic intensities were 0.111, 0.167, 0.222, 0.278, and 0.694 W/cm^2 respectively, and the acoustic pressures were 46, 56, 65, 73, and 115 kPa respectively. Mechanical stirring of 30 W with a rotation rate of 900 revolutions per minute (rpm) was also applied during the process. The temperature was controlled at a constant of 60 °C The reaction lasted for 15 min. The initial pH values of the solutions were measured as 5.8 ± 0.2. After different ultrasonic treatments, the final pH values of these solutions were all measured as 3.3 ± 0.2. Once the reaction was accomplished, Cu nanoparticles were extracted from the solution via centrifugation at 12,000 rpm for 2 min. The Cu nanoparticles were cleaned with ethanol and deionized water in turn for three times, and then dried in vacuum for 3 h for use. The morphology of the as-synthesized Cu nanoparticles was characterized by a field-emission scanning electron microscope (FESEM, Hitachi SU8220). The size distribution was measured by a laser particle size analyzer (Mastersizer 3000, Malvern, England).

3. Results and discussion

Fig. 1 shows the SEM morphologies of the as-synthesized Cu nanoparticles under different ultrasonic powers. It can be observed that the as-synthesized Cu nanoparticles are roughly in spherical shape. After ultrasonic treatment, the size of the nanoparticles is significantly reduced, and the morphologies become more regular and consistent. The XRD patterns of the as-synthesized Cu nanoparticles under different ultrasonic irradiation powers are provided in the Supplementary material. From the XRD patterns, only the peaks of crystallite Cu can be observed, without any peaks of oxides.

The size distribution of the Cu nanoparticles under different ultrasonic powers was measured by a particle size analyzer, and the statistical results are shown in Fig. 2 and Table 1. As the ultrasonic power increases from 0 to 500 W, the average diameter of the Cu nanoparticles decreases from 520 to 167 nm, and the size dispersion also decreases from 94 to 44 nm.

According to the full width at half maximum (FWHM) of the XRD patterns, the crystallite size of the as-synthesized Cu nanoparticles under different irradiation powers were calculated based on Debye-Scherrer formula and summarized in Table 2. It can be found that the average crystallite size falls in the range of 25–30 nm and is not sensitive to the ultrasonic irradiation power. This implies that the influence of ultrasound on the nucleation and growth process of the Cu crystallites is relatively weak under the conditions in this study. Hence, the size refinement of the Cu particles under ultrasound treatment is probably attributed to the prevention effect of ultrasound on the aggregation of crystallites, rather than the size reduction of the crystallites themselves.

The above results show a clear decreasing trend of particle size with increasing ultrasonic power, which agrees well with the observation of many previous studies [7,19,21]. Here we propose a model to understand the relationship between the particle size and the ultrasonic power. The increase in particle size can be achieved via continuous growth of a particle or gradual aggregation of different particles. For the aggregation of different particles, the contact of particles can reduce the total surface area, thereby reducing the overall energy. Fig. 3(a) illustrates this process through a two-particle model. Assume that the radius of the two particles is R and that the two particles form a circular contact surface with a center angle of 2θ. Then the circumference of the circular contact surface is $2\pi R\theta$. Due to the surface energy of the particles, there will be a tension force at the edge of the contact surface, which can be expressed as

$$F_s = 2\pi\theta R\gamma \tag{1}$$

where γ represents the surface energy of the metal particle.

On the other hand, due to the contact of the two particles, a part of the spherical cap of the particles is flattened, and there will be a compressive strain near the contact surface. The magnitude of the strain can be approximately estimated according to the ratio of the height of the original spherical cap to the radius of the particle, with the expression of

$$\varepsilon = \frac{1}{R}\left(\frac{R\theta^2}{2} - \frac{R\alpha^2}{2}\right) = \frac{\theta^2}{2} - \frac{\alpha^2}{2} \tag{2}$$

where α represents the center angle at a given position on the contact surface. By integrating the stress on the entire contact surface based on the above strain, the total pressure can be obtained as

$$F_C = \int_0^{\theta} \pi R^2 E\left(\theta^2 - \alpha^2\right)\alpha d\alpha = \frac{\pi R^2 E\theta^4}{4} \tag{3}$$

where E represents the elastic modulus of the metal particle.

According to Eqs. (1) and (3), the total tensile force between the two particles can be expressed as $F_T = F_s - F_c$. At $\theta = (2\gamma/ER)^{2/3}$, the total tensile force can reach a maximum of

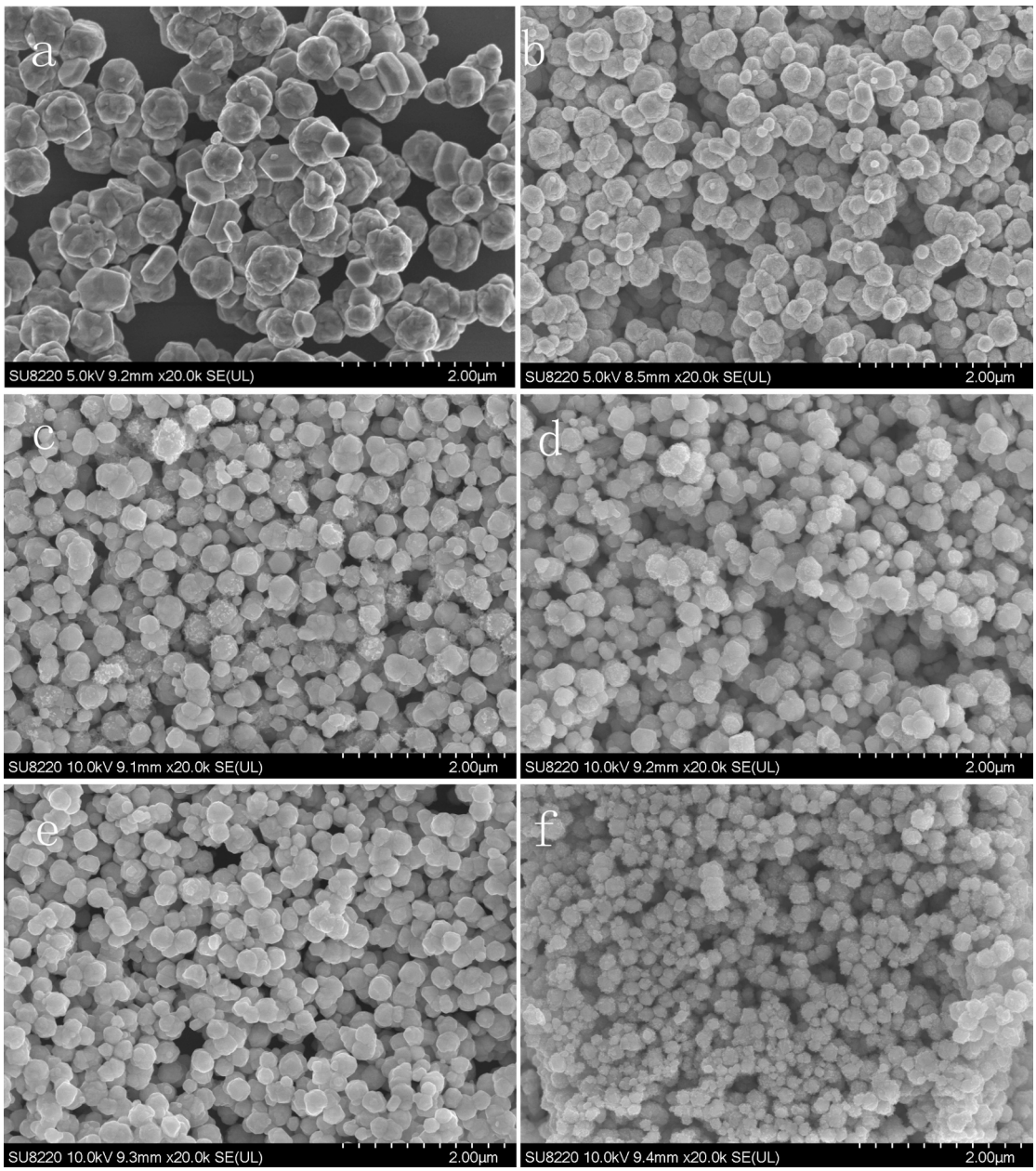

Fig. 1. SEM morphologies of the as-synthesized Cu nanoparticles under different ultrasonic powers of (a) 0 W, (b) 80 W, (c) 120 W, (d) 160 W, (e) 200 W, and (f) 500 W.

$$F_T = \frac{3}{2^{2/3}}\pi E^{-\frac{1}{3}} R^{\frac{2}{3}} \gamma^{\frac{4}{3}} = 5.94 E^{-\frac{1}{3}} R^{\frac{2}{3}} \gamma^{\frac{4}{3}} \tag{4}$$

Eq. (4) represents the required force to separate the particles. Under ultrasound conditions, the applied ultrasound can induce surface tension between the particles. For a planar standing wavefield, the acoustic radiation force (F_r) on a compressible spherical particle can be expressed as [23,24]:

$$F_r = -\frac{2\pi^2 p_0^2 R^3 \beta_l}{3\lambda} \Phi sin(2kx) \tag{5}$$

where p_0 is the pressure amplitude, β_l is the compressibility of the liquid and equals $\beta_l = 1/\rho_l c_l^2$, ρ_l is the density of the liquid, c_l is the acoustic wavespeed in the liquid, k is the wavenumber and equals $2\pi/\lambda$, and Φ can be calculated by

$$\Phi = \frac{5\rho_p - 2\rho_l}{2\rho_p + \rho_l} - \frac{\beta_p}{\beta_l} \tag{6}$$

where ρ_p is the density of the particle and β_p is the compressibility of the particle.

Considering that the square of the pressure amplitude is proportional to the power of ultrasonic power, Eq. (5) can be rewritten as

$$F_{rmax} = APR^3 \tag{7}$$

where P represent the ultrasonic power, and A is a constant under the same reaction condition.

When the tensile force exceeds the maximum tensile force between the two particles ($F_{rmax} > F_T$), the two particles will be separated. The critical particle size can be determined by $F_{rmax} = F_T$, which gives

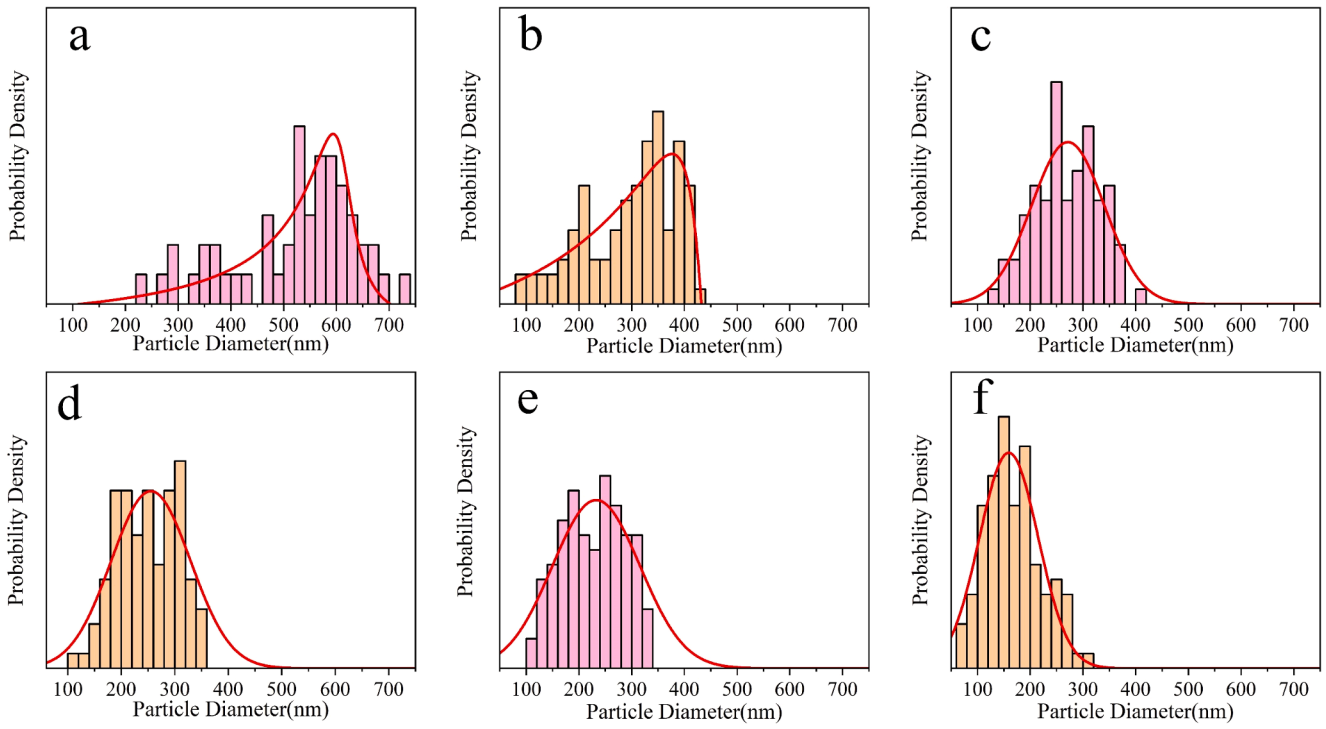

Fig. 2. Size distribution of the as-synthesized Cu nanoparticles under different ultrasonic powers of (a) 0 W, (b) 80 W, (c) 120 W, (d) 160 W, (e) 200 W, and (f) 500 W.

Table 1
Statistics of the size distribution of the as-synthesized Cu nanoparticles under different ultrasonic powers.

Irradiation power (W)	Ultrasonic intensity (W/cm^2)	$pH_{initial}$	pH_{final}	Average diameter (nm)	10% (nm)	50% (nm)	90% (nm)	Dispersion (nm)
0	0	5.8 ± 0.2	3.3 ± 0.2	520	339	546	647	94
80	0.111			298	173	319	397	69
120	0.167			266	193	263	348	56
160	0.222			247	177	246	319	47
200	0.278			226	148	230	303	50
500	0.694			167	102	161	246	44

Table 2
Average crystallite size of the as-synthesized Cu nanoparticles under different irradiation powers.

Irradiation Power (W)	Crystallite Size (nm)
0	29.1
80	24.6
120	27.3
160	27.3
200	24.6
500	25

$$R_c = \left(\frac{27\gamma^4}{4A^3EP^3}\right)^{\frac{1}{7}} \propto \gamma^{\frac{4}{7}} P^{-\frac{3}{7}} \tag{8}$$

Eq. (8) provides a relational expression for determining the critical size of metal particles under ultrasonic treatment. The particles with $R < R_c$ can grow through aggregation with each other, while the aggregation of the particles with $R > R_c$ can be prevented by the acoustic radiation force from the ultrasound. This effect reduces the number of large particles in the solution and reduces the dispersion of particle size.

Fig. 3(b) shows the relationship between the logarithms of particle size and ultrasonic power. Here, considering the stirring effect, we take an equivalent ultrasonic power of $P = P_0 + P_s$ as the nominal ultrasonic power, where P_0 represents the ultrasonic power and P_s = 30 W represents the equivalent stirring power. It can be seen that there is an obvious linear relationship of $d \propto P^{-0.395}$, with a coefficient of determination (COD) of $R^2 = 0.9733$. This relation is basically consistent with the prediction of Eq. (8).

The above model well explains the relationship between the particle size and the ultrasonic power during the synthesis of metal nanoparticles, and it is in good agreement with the experimental results. As the model indicates, the particle size is proportional to the ultrasonic power to the power of −0.395 ($d \propto P^{-0.395}$). Hence, the size of the particles decreases with increasing ultrasonic power. However, when a large enough ultrasonic power is applied, the decreasing trend of $P^{-0.395}$ slows down. In the meantime, the energy provided by the increase in ultrasonic power may promote the continuous growth of the particles. As a result, further increase in ultrasonic power cannot enhance particle refinement but may increase the particle size, which explains many previously reported experimental results [11,21].

On the other hand, the model also indicates that the particle size is affected by the surface energy (γ). The surface energy of the Cu nanoparticles is $\gamma_{Cu(1\,1\,1)} = 1.83$ J/m^2 [25]. By reducing the surface energy, the particle size can be refined. Dispersants are commonly used additives in the synthesis of nanoparticles [19,20]. When the dispersants are adsorbed on the surface of nanoparticles, they can change the surface properties of the nanoparticles, and equivalently reduce their surface energy.

The model in this study provides a quantitative relationship between

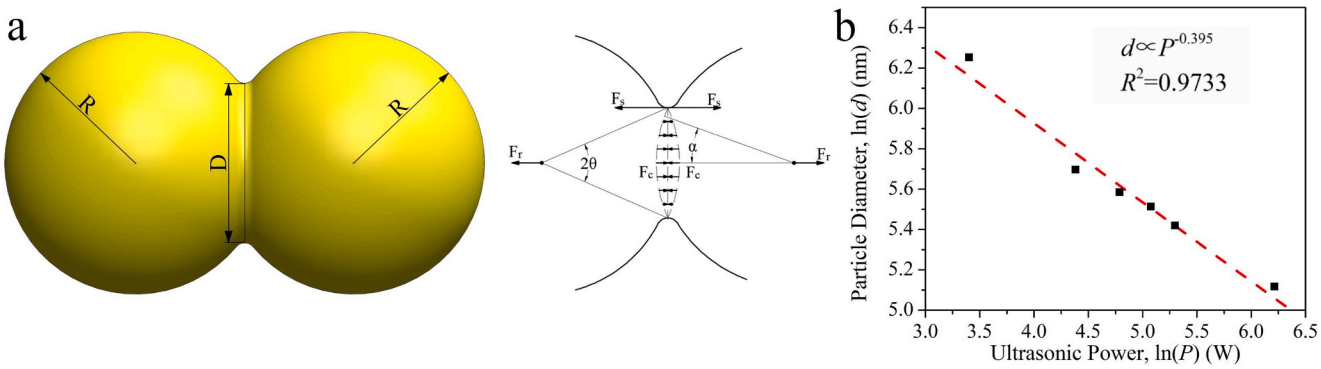

Fig. 3. (a) Schematic diagram of the two-particle model; (b) relationship between the logarithms of particle size and ultrasonic power.

particle size and ultrasonic power in the synthesis of metal nanoparticles. However, the ultrasonic intensity under the applied ultrasonic power of 500 W is 0.694 W/cm^2, and the corresponding ultrasound pressure is only 115 kPa. These values are relatively low compared to the ultrasonic intensity/pressure in previous studies [26–28]. The minimum pressure of cavitation threshold in water is expected to be 500 kPa [29] or 100–200 kPa [30]. Therefore, the applied ultrasonic intensity in this study is not high enough to induce an obvious cavitation effect. Above the cavitation threshold, the cavitation effect may have some additional effects on the de-aggregation of particles. For example, some studies have revealed that when bubbly clouds are generated, the shielding and scattering effects of the bubbly clouds can drastically reduce the emitted acoustic pressure levels travelling through the liquid media, thus significantly weakening the ultrasound field outside the conical bubble structure [28,31]. The collapse and rebound of a cavitation bubble can produce strong shock waves and extremely high pressure [26]. In liquid aluminum, the pressure of the shock waves can reach the order of Megapascal [27,32,33]. These effects can promote the fragmentation and de-aggregation of the particles. The temporal and spatial relationships of the ultrasound-induced shock waves and acoustic pressure emissions are complicated and still need further study.

4. Conclusions

In this study, the evolution of size distribution of Cu nanoparticles synthesized via the wet-chemical redox method under ultrasonic treatment was statistically analyzed. With increasing ultrasonic power from 0 to 500 W, the average diameter of the Cu nanoparticles decreased from 520 to 167 nm, and the size dispersion decreased from 94 to 44 nm. A model was proposed to quantitatively describe the influence of ultrasonic power on the size distribution of metal nanoparticles from the perspective of the competition between the surface energy and the ultrasonic force. An exponential relation of $R_c \propto \gamma^{\frac{4}{7}} P^{-\frac{3}{7}}$ was established, and it fitted well with the experimental results. The results and the proposed model in this study provide new experimental basis and theoretical method for understanding the mechanism of ultrasonic-induced size refinement of metal nanoparticles during their synthesis process.

CRediT authorship contribution statement

Guannan Yang: Conceptualization, Investigation, Methodology, Writing - original draft, Writing - review & editing. **Wei Lin:** Investigation, Data curation, Visualization. **Haiqi Lai:** Investigation. **Jin Tong:** Investigation. **Junjun Lei:** Methodology. **Maodan Yuan:** Methodology. **Yu Zhang:** Supervision, Funding acquisition. **Chengqiang Cui:** Supervision, Funding acquisition.

Declaration of Competing Interest

The authors declare that they have no known competing financial interests or personal relationships that could have appeared to influence the work reported in this paper.

Acknowledgements

This work is supported by the National Natural Science Foundation of China (Grant Nos. 61874155 and 61704033) and the National Key R&D Program of China (Grant No. 2018YFE0204601).

Appendix A. Supplementary data

Supplementary data to this article can be found online at https://doi.org/10.1016/j.ultsonch.2021.105497.

References

[1] C. Wang, G.J. Xiao, Y.M. Sui, X.Y. Yang, G. Liu, M.J. Jia, W. Han, B.B. Liu, B. Zou, Synthesis of dendritic iridium nanostructures based on the oriented attachment mechanism and their enhanced CO and ammonia catalytic activities, Nanoscale 6 (2014) 15059–15065.
[2] V. Zin, S. Barison, F. Agresti, L. Colla, C. Pagura, M. Fabrizio, Improved tribological and thermal properties of lubricants by graphene based nano-additive, RSC Adv. 6 (2016) 59477–59486.
[3] H. Yamamoto, H. Yano, H. Kouchi, Y. Obora, R. Arakawa, H. Kawasaki, N,N-Dimethylformamide-stabilized gold nanoclusters as a catalyst for the reduction of 4-nitrophenol, Nanoscale 4 (2012) 4148–4154.
[4] R.C. Jin, Atomically precise metal nanoclusters: stable sizes and optical properties, Nanoscale 7 (2015) 1549–1565.
[5] K. Bramhaiah, S.S. John, Hybrid films of reduced graphene oxide with noble metal nanoparticles generated at a liquid/liquid interface for applications in catalysis, RSC Adv. 3 (2013) 7765–7773.
[6] A.J. Biacchi, R.E. Schaak, Ligand-induced fate of embryonic species in the shape-controlled synthesis of rhodium nanoparticles, ACS Nano 9 (2015) 1707–1720.
[7] L. Shi, Z. Zhang, R. Wang, C. Zhou, C. Sun, Study on ultrasound-assisted precipitation for preparing Ni/Al_2O_3 catalyst, Ultrason. Sonochem. 67 (2020), 105107.
[8] M. Li, Y. Xiao, Z. Zhang, J. Yu, Bimodal sintered silver nanoparticle paste with ultrahigh thermal conductivity and shear strength for high temperature thermal interface material applications, ACS Appl. Mater. Interfaces 7 (2015) 9157–9168.
[9] S. Murchio, Y. Ding, G. Speranza, G.D. Sorarù, D. Maniglio, Ultrasound-assisted hydroxyapatite-decorated breath-figure polymer-derived ceramic coatings for Ti_6Al_4V substrates, ACS Appl. Mater. Interfaces 12 (2020) 50772–50783.
[10] J. Nampoothiri, R.S. Harini, S.K. Nayak, B. Raj, K.R. Ravi, Post in-situ reaction ultrasonic treatment for generation of Al-4.4Cu/TiB_2 nanocomposite: a route to enhance the strength of metal matrix nanocomposites, J. Alloy. Compd. 683 (2016) 370–378.
[11] P.A. Bozkurt, Sonochemical green synthesis of Ag/graphene nanocomposite, Ultrason. Sonochem. 35 (2017) 397–404.
[12] M. Mousavi-Kamazani, Facile sonochemical-assisted synthesis of Cu/ZnO/Al_2O_3 nanocomposites under vacuum: optical and photocatalytic studies, Ultrason. Sonochem. 58 (2019) 10.
[13] W. Lv, Z. Luo, H. Yang, B. Liu, J.J.U.S. Liu, Effect of processing conditions on sonochemical synthesis of nanosized copper aluminate powders, Ultrason. Sonochem. 17 (2010) 344–351.
[14] D.W. Inglis, R. Riehn, R.H. Austin, J.C. Sturm, Continuous microfluidic immunomagnetic cell separation, Appl. Phys. Lett. 85 (2004) 5093–5095.

[15] M. Kersaudy-Kerhoas, R. Dhariwal, M.P.Y. Desmulliez, Recent advances in microparticle continuous separation, IET Nanobiotechnol. 2 (2008) 1–13.
[16] Y. Li, K.V.I.S. Kaler, Dielectrophoretic fluidic cell fractionation system, Anal. Chim. Acta 507 (2004) 151–161.
[17] P. Pujar, K.K.M. Jagadeeshkumar, M. Naqi, S. Gandla, H.W. Cho, S.H. Jung, H. K. Cho, J.T. Kalathi, S. Kim, High-intensity ultrasound-assisted low-temperature formulation of lanthanum zirconium oxide nanodispersion for thin-film transistors, ACS Appl. Mater. Interfaces 12 (2020) 44926–44933.
[18] Y. Zhang, R. Di, H. Zhang, W. Zhang, C. Yang, Effective recovery of casein from its aqueous solution by ultrasonic treatment assisted foam fractionation: inhibiting molecular aggregation, J. Food Eng. 284 (2020), 110042.
[19] Y. Zhao, Q. Zheng, Z. Liu, Ultrasound-induced distribution of nano-sized TiB_2 particles within α-Al grains during solidification of Al-7Si alloy, Mater. Lett. 274 (2020), 128030.
[20] P. Christy Roshini, B. Nagasivamuni, B. Raj, K.R. Ravi, Ultrasonic-assisted synthesis of graphite-reinforced Al matrix nanocomposites, J. Mater. Eng. Perform. 24 (2015) 2234–2239.
[21] S.S. Sabnis, R. Raikar, P.R. Gogate, Evaluation of different cavitational reactors for size reduction of DADPS, Ultrason. Sonochem. 69 (2020), 105276.
[22] J. Amaro-Gahete, A. Benitez, R. Otero, D. Esquivel, C. Jimenez-Sanchidrian, J. Morales, A. Caballero, F.J. Romero-Salguero, A comparative study of particle size distribution of graphene nanosheets synthesized by an ultrasound-assisted method, Nanomaterials 9 (2019) 152.
[23] W.T. Coakley, D.W. Bardsley, M.A. Grundy, F. Zamani, D.J. Clarke, Cell manipulation in ultrasonic standing wave fields, J. Chem. Technol. Biotechnol. Biotechnol. 44 (1989) 43–62.
[24] P.L.M.J. van Neer, A. Rasidovic, A.W.F. Volker, Ieee, A study of nanoparticle manipulation using ultrasonic standing waves, in: IEEE International Ultrasonics Symposium, 2013, pp. 1915–1918.
[25] H.L. Skriver, N.M. Rosengaard, Surface energy and work function of elemental metals, Phys. Rev. B: Condens. Matter 46 (1992) 7157–7168.
[26] D.G. Eskin, I. Tzanakis, F. Wang, G.S.B. Lebon, T. Subroto, K. Pericleous, J. Mi, Fundamental studies of ultrasonic melt processing, Ultrason. Sonochem. 52 (2019) 455–467.
[27] G.S.B. Lebon, K. Pericleous, I. Tzanakis, D.G. Eskin, Dynamics of two interacting hydrogen bubbles in liquid aluminum under the influence of a strong acoustic field, Phys. Rev. E 92 (2015) 8.
[28] I. Tzanakis, M. Hodnett, G.S.B. Lebon, N. Dezhkunov, D.G. Eskin, Calibration and performance assessment of an innovative high-temperature cavitometer, Sens. Actuators A: Phys. 240 (2016) 57–69.
[29] V.S. Moholkar, S.P. Sable, A.B. Pandit, Mapping the cavitation intensity in an ultrasonic bath using the acoustic emission, AIChE J. 46 (2000) 684–694.
[30] K. Yasui, Acoustic Cavitation, Acoustic Cavitation and Bubble Dynamics, Springer, 2018, pp. 1–35.
[31] I. Tzanakis, G.S.B. Lebon, D.G. Eskin, K.A. Pericleous, Characterizing the cavitation development and acoustic spectrum in various liquids, Ultrason. Sonochem. 34 (2017) 651–662.
[32] A. Priyadarshi, M. Khavari, T. Subroto, M. Conte, I. Tzanakis, On the governing fragmentation mechanism of primary intermetallics by induced cavitation, Ultrason. Sonochem. 70 (2020), 105260.
[33] I. Tzanakis, G.S.B. Lebon, D.G. Eskin, K.A. Pericleous, Characterisation of the ultrasonic acoustic spectrum and pressure field in aluminium melt with an advanced cavitometer, J. Mater. Process. Technol. 229 (2016) 582–586.